Nanostructured (Ti,Cu)N Dry Electrodes for Advanced Control of the Neuromuscular Activity

Cláudia Lopes, Hugo Veloso, Makenna Hayes, Michael A. Cullinan, *Member, IEEE*, and Filipe Vaz

***Abstract*—This research reports a novel concept of dry surface electrodes designed to act in a dual-role biofeedback process: monitoring and stimulating the muscle's electrical activity. A new strategy based on 3-D printed polymeric disk-shaped substrates functionalized with nanostructured (Ti,Cu)N thin films to be integrated into rehabilitation wearables. Five different chemical compositions with different microstructural features were grown by dc magnetron sputtering on polyurethane (PU), polylactide, and cellulose polymers and tested as electrodes. In the first phase, the electromyography (EMG) activity for both resting and muscle contraction of the bicep muscle was assessed using the LabVIEW software coupled to a NI 9234 signal data acquisition system and processed with MATLAB algorithms. The second phase tested the maximum electrical stimulation capable of being delivered without crosstalking between stimulation and sensing processes, using a TENS 7000 commercial unit. The tests highlighted the potential of the flexible PU bases among their counterparts, whereas the dense and soft electrodes of titanium doped with 25.6.% of copper were able to stimulate at a 100-mA full current output without discomfort for the subject exhibiting simultaneously the lowest EMG detection limit. The research conducted enhances the strong potential of using dry electrodes in new technologies and strategies capable of delivering primary and integrated care adapted to foster functional abilities.**

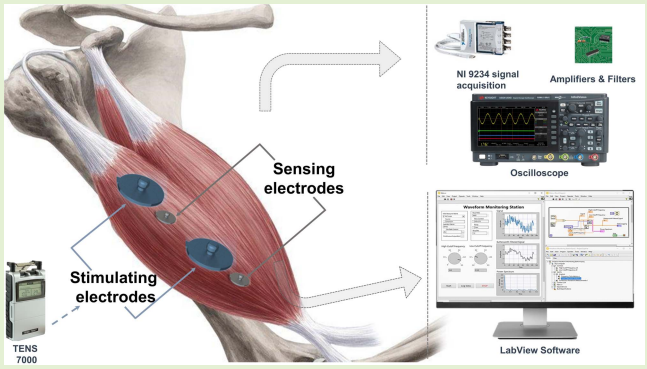

***Index Terms*— Dry electrodes, electrical stimulation, electromyography (EMG), nanostructured thin films, rehabilitation.**

I. Introduction

THE world's population is aging. According to the most recent report from the United Nations (UN) and the World Health Organization (WHO), the number of older persons worldwide (aged 65 years or over) is projected to reach over 1.5 billion in 2050, an increase from 9.3% in 2020 to around 16% in 2050 [1]. As the population ages, the necessity of long-term care takes more relevance and the pressure on healthcare centers begins to reach alarming levels [2], [3], [4]. Several political, social, and economic measures need to be rethought, to prepare an adequate response of the health systems to the aging population shift. Global awareness of all the social and economic sectors is fundamental to allow better coordination of care across health and social services, as well as to provide conditions for more treatments out of the hospital.

The UN has proclaimed 2021–2030 the decade of healthy aging, with WHO leading international action to improve the lives of older people and their families and communities, promote the rehabilitation of health systems, and establish environments that guarantee economic well-being as well as physical and psychosocial health and life satisfaction of the elderly population [5].

Regarding healthcare concerns and therapies, it is important to mention that the majority of the medical routines, namely, diagnostic exams or rehabilitation treatments, are exclusively performed in healthcare centers, leading patients to travel to the facilities. These trips are increasingly a problem due to the rise in the incidence of musculoskeletal conditions in the global population, the biggest contributor to disability worldwide. This problem is even more acute for the elderly

Manuscript received 13 October 2022; revised 14 December 2022; accepted 19 December 2022. Date of publication 4 January 2023; date of current version 13 February 2023. This work was supported by the European Regional Development Fund (ERDF) through the Operational Programme for Competitiveness and Internationalization (COMPETE 2020) under Portugal 2020 in the framework of the NanoStim Project under Grant POCI-01-0247-FEDER-045908 and the NanoID Project under Grant NORTE-01-0247-FEDER-046985. The associate editor coordinating the review of this article and approving it for publication was Prof. Minhee Yun. *(Corresponding author: Michael A. Cullinan.)*

This work involved human subjects or animals in its research. The authors confirm that all human/animal subject research procedures and protocols are exempt from review board approval.

Cláudia Lopes, Hugo Veloso, and Filipe Vaz are with the Physics Center of Minho and Porto Universities (CF-UM-UP), Universidade do Minho, 4710-057 Braga, Portugal (e-mail: claudialopes@fisica.uminho.pt).

Makenna Hayes and Michael A. Cullinan are with the Department of Mechanical Engineering, The University of Texas at Austin, Austin, TX 78712 USA (e-mail: michael.Cullinan@austin.utexas.edu).

Digital Object Identifier 10.1109/JSEN.2022.3232264

population, which is the demographic group most affected by musculoskeletal conditions, directly limiting their mobility, and dexterity and making it difficult or even impossible for the elderly to perform routine activities [6], [7], [8]. In this respect, it is widely accepted that the treatment of disabilities is projected to grow, and as a result, the burden on healthcare services may increase.

One advantage of home-based physiological monitoring systems is that constant oversight by healthcare professionals is not needed, and care may be assessed by each patient. Over the past few decades, noninvasive physiological monitoring technology has made a considerable impact on medical diagnostics and personal healthcare using imaging and electrical sensing technology. Typical signals processed through imaging and electrical sensing include the heart rate, muscle current, and brain electrical activity. An example of a beneficial home-based electrical sensing monitoring technology is the telemonitoring of heart failure patients. By monitoring ventricular arrhythmias, heart rate variability, and changes in the electrocardiographic traces, patients and healthcare workers can easily observe these parameters and greatly benefit [9].

With respect to available solutions for physiological monitoring technologies, gel-based/wet electrodes of Ag/AgCl are widely used on surface electromyographic (sEMG) measurements. However, despite its advantages, such as low polarization effect, low electrode–skin interface impedance, low cost, and ease of use [10], [11], [12], this type of electrode has several disadvantages, such as the use of a moist environment that for prolonged use can lead to allergic reactions and skin irritations, which together with the drying of the medium reduce the comfort of use. In this way, dry electrodes represent the opportunity to carry out electromyography (EMG) monitoring at home, as they are reusable, comfortable, less costly, and easy to use while still being able to obtain signals comparable to wet electrodes [10], [11], [12]. This remote analysis can be performed using a garment equipped with strategically placed acquisition electrodes to record the desired muscles.

In this study, a new system of dry electrodes based on flexible polymers functionalized with biocompatible thin films was investigated. For this, five different combinations of (Ti,Cu)N thin films were selected (Ti, Cu, TiN, TiCu, and TiNCu), to functionalize polyurethane (PU), organic cellulose, and polylactide (PLA) polymeric substrates. Titanium (Ti) was chosen due to its medical properties, such as biocompatibility with human tissue, corrosion resistance, and excellent wear, as well as due to its excellent thermal and chemical stability, elasticity, and strength [11], [12], [13]. Titanium nitride (TiN) was also considered due to its biocompatibility, good mechanical properties, good conductivity, easiness of processing, and chemical resistance when in contact with sweat. The addition of Cu to TiN thin films is due to its excellent electrical properties, as well as its low toxicity, high cytocompatibility, and the fact that it is a metabolizing agent, i.e., Cu is naturally removed by the body when released into it [14], [15]. The use of the films prepared to sense the electrical activity of the muscles is reported in the following.

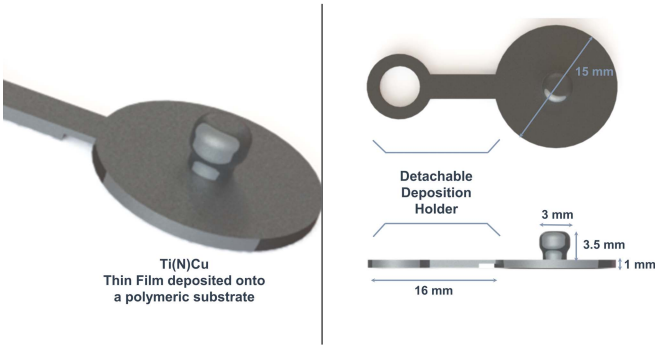

Fig. 1. Dry electrode's conception is based on 3-D printed polymeric substrates functionalized with (Ti,Cu)N thin films for surface EMG monitoring.

II. Preparation of (Ti,Cu)N Surface Dry Electrodes

The dry electrodes for surface EMG were prepared through the deposition of nanometric thin films of Ti and TiN, doped with copper (TiCu and TiNCu) onto polymeric substrates. The depositions were carried out using a custom-made dc magnetron sputtering system [11], [12], [13].

The polymeric substrates were 3-D printed via fused deposition modeling (FDM) using a 3-D printer (ZMorph model VX) and filaments of biodegradable polylactic acid, PLA (Eastman Amphora AM3300, Kingsport, TN, USA), sustainable cellulose nanofibrils (FILAMENTIVE, Batch 840620, diameter 1.75 mm, Bradford, U.K.), and flexible PU (SMARTFILL, FLEX Lot Code 155264002953, diameter 1.75 mm, Alcalá la Real, Jaén, Spain)

Disk-shaped bases with a snap connection were designed to be 3-D printed and used as dry electrode substrates. The snap button guarantees a stable and reliable electronic connection with shielded snap leads, working at the same time as an active fixing point in the wearable. Technical details of the electrode may be consulted in Fig. 1. Before the deposition process and to optimize the adhesion of the (Ti,Cu)N films on the 3-D printed polymers, the substrates were cleaned with ethanol and activated by plasma treatments [11], [12], [16]. A Diener plasma cleaner system (Plasma System Zepto, Diener electronic GmbH & Company KG, Ebhausen, Germany) with a 13.56-MHz generator connected to a rotary pump working at a low base pressure of 20 Pa was used. Different atmospheres (Ar, O_2, N_2, Ar + O_2, and Ar + N_2) at the maximum power of 50 W during (1, 3, 5, and 15 min) were employed. All plasma treatments were conducted with a constant working pressure of 100 Pa. The extent of activation promoted on the substrate's surface was tested in terms of wettability since the higher the surface energy (SE) of the substrates, the better the adhesion [16], [17]. SE analysis on postactivated polymeric surfaces was determined at room temperature, by measuring the contact angle (CA) of different liquids: 1) ultrapure water; 2) glycerol (99.5%, Biochem); and 3) 1-bromonaphthalene (>95%, Frilabo) using a CA goniometer (OCA 15, DataPhysics Instruments GmbH, Filderstadt, Germany). A minimum of three valid sessile drop repetitions were performed for each liquid and plasma condition. The SE of each activated polymer was analyzed with Phyton

(version 3.9.1) programming language applying the Fowkes method [18], [19].

The most promising plasma treatments were used to activate the polymeric bases, immediately before being deposited with the five different types of films within the (Ti,Cu)N system. The thin films were deposited by dc magnetron sputtering at very low pressures ($<7.0 \times 10^{-4}$ Pa). The discharge voltage was generated using a dc power supply (a current density of 75 A/m^2) in a pure Ar atmosphere for the deposition of the Ti/Cu-based thin films and in a reactive mixed gas atmosphere ($Ar + N_2$) for the TiN-based ones. The Ar flow (25 sccm) was kept constant for all depositions, while the flow rate of nitrogen was fixed at 2.5 sccm for the TiN depositions, and the work pressure was around 3.0×10^{-1} Pa. All the thin films were prepared with a grounded planetary substrate holder centered inside the vacuum chamber, distanced 70 mm from the target, to guarantee a homogeneous deposition. This substrate holder moved in a rotation mode at a constant speed of 5.5 r/min relative to the target, while the samples spin around the axis supporting them, mimicking the motion of the planets in the solar system. Two different targets were used, one of Cu (99.99%, 200 × 100 × 6 mm) to prepare a pure Cu thin film and the other of pure Ti (99.99 % purity) for all the other depositions. To prepare the TiCu and TiNCu thin films, the Ti target was modified with 25 metallic pellets of Cu (area: 16 mm^2 and thickness: 0.5 mm) glued with conductive silver glue onto the erosion zone of the Ti target. All depositions were performed at room temperature for times no longer than 20 min to avoid the polymer's thermal degradation [16], [20] aiming to achieve the same film's thicknesses (∼250 nm).

The chemical composition of the as-deposited films was assessed by the Rutherford backscattering spectrometry (RBS) analysis. The analysis was performed inside a small RBS chamber, where monoenergetic and collimated beams of ions $4He^+$ and/or $1H^+$ were accelerated by a Van der Graaf accelerator with approximately 2.5 MeV, colliding perpendicularly with the surface of the sample (normal incidence). The backscattered ions were recorded using three detectors positioned inside the chamber: one at 140° scattering angle for Si surface barrier detection and two pin-diode detectors positioned symmetrically to each other at 165°, both on the same side. The NDF software was used for the simulation of the in-depth composition profiles of each sample, using three different measurements [21], [22].

The morphological features of the thin films were evaluated using a high-resolution scanning electron microscope (SEM; FEI Nova NanoSEM 200) with X-ray microanalysis and electron backscattered diffraction analysis, operating at 15 keV. Cross-sectional micrographs were used to determine the thickness of the films and top-view images to evaluate the topography.

III. Characteristics of the Electrodes

A. Polymeric Substrates

The optical CA and SE of the untreated and plasma-treated polymeric bases were evaluated for high polar (water), median polar, and dispersive (glycerol) ad high dispersive (bromonaphthalene) liquids on the surface of the polymeric bases, using the sessile drop technique and applying the Fowlkes method. The results are presented in Fig. 2, considering the different plasma treatments performed. Only 1 min of exposure to a plasma atmosphere was sufficient to improve the wettability by no less than 28% of all the polymeric bases. The water CA falls from ∼107.0° for untreated PU bases to ∼76.4° after activation with Ar plasma, reaching the minimum of ∼31.7° into a mixed atmosphere of Ar and O_2. Identical behavior is observed for the PLA and cellulose polymers. Nevertheless, the wettability of the polymeric bases is enhanced if the duration of the plasma treatment increases, especially evident for the cellulose bases. At the same time, a significant improvement of at least 27.8% (corresponding to argon plasma treatment) was observed on the SE of the polymers exposed to plasma for 1 min, regardless of the atmosphere used.

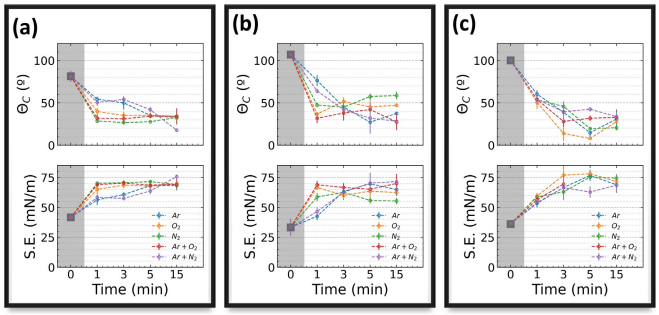

Fig. 2. Evolution of the water CA of the different polymeric bases: (a) PLA, (b) PU, and (c) cellulose. The SE was calculated using the Fowkes method.

The water CA reduction and consequent increase of the SE values may be closely related to changes on the surface topography, by cleaning contaminants and etching the polymer's surface, but also by promoting the formation of new oxygen- and/or nitrogen-containing polar functional groups [16], [17], [23].

The results also show that plasma treatments carried out for periods longer than 5 min did not significantly influence the activation of the polymers. For the PLA bases treated for 15 min, an increase of less than 10% in the mean SE values was obtained; for PU bases, no significant changes were noticed, whereas for cellulose, a slight decrease without statistical significance (considering the error bars) was observed. It seems that after 5 min and especially on cellulose, the treatments lead to further etching and to the ablation of the polar groups obtained for shorter periods, reversing the intended effect of the plasma treatment [24].

The physical adhesion of the (Ti,Cu)N thin films to the polymers significantly increases for better wettability and higher SE values since the intermolecular interactions at the interface are enhanced. Based on the results, the most promising treatments were selected, for each polymeric base to be performed before each deposition.

Considering the PU bases, the selected atmosphere was Ar by 5 min since the water CA reached the minimum value of ∼27.2°, improving the wettability by 74.6%. In the same way, the SE of the untreated surfaces doubled, increasing from 33.3 to 69.8 mN/m. As reported in other works [16], [25],

TABLE I
CHEMICAL COMPOSITION OF (Ti,Cu)N THIN FILMS

Thin Film	Ti (at.%)	N (at.%)	Cu (at. %)
Ti	100	-	-
TiN	53.6	46.4	-
TiCu	74.4	-	25.6
TiNCu	34.4	34.4	31.2
Cu	-	-	100

despite the physical changes, the Ar ions could break/split the chemical bonds of C–O and C=O promoting the formation of free radicals (dangling bonds) able to strengthen the bonding with the metallic elements of the thin film improving the adhesion.

The maximum activation of PLA bases was achieved in a mixed Ar + N_2 plasma carried out for 15 min at 50 W. The wettability increased by ∼78% (reduction in the water CA from 81.4° for the untreated sample to 17.6° after activation) and the SE was enhanced by 72%, increasing from 41.6 to 71.6 mN/m. In addition to the physical etching and ablation effects promoted by the bombardment with Ar^+ ions, the use of N_2 gas promotes the introduction of nitrogen-containing functional groups on the polymer's surface, such as amine ($-NH_3$) and imine ($R_2C{=}NR$) groups, improving the surface hydrophilicity and increasing the ability to establish new bonds with metallic elements [26], [27], [28].

Regarding the bases of cellulose, the maximum surface wettability and energy were reached for an O_2 plasma of 5 min. Relative to the untreated polymer, the water CA dropped to the minimum value of ∼7.9°, which means that the hydrophilicity of the samples increased by about 92%, and the SE raised from 36.11 to 78.77 mN/m, relatively to the untreated polymer. For cellulose, the reactive nature of an O_2 plasma seems to play a determining role in the formation of oxygen-containing species that may later favor the adhesion of the deposited thin film. In addition, the O_2 plasma is also responsible for etching the surface by changing the roughness and contributing to an increase in mechanical interlock at the interface with the film [16], [24], [25].

B. Thin Films—Chemical Composition and Morphology

The chemical composition was determined by the RBS spectral analysis and is presented in Table I, relating the percentages of each element in the different films prepared.

As expected, the pure Ti and Cu thin films contain 100% of the respective element. In the same vein, TiN-based thin films were prepared in stoichiometric conditions since Ti and N coexist in similar atomic percentages. The TiCu thin films were prepared in a 1:3 (Cu/Ti) ratio, and for this composition and in agreement with the authors' previous works [13], [17], the formation of intermetallic bonds prevails. Regarding the TiNCu films, all the elements exist in the same proportion, 31.2% of Cu doping a stoichiometric TiN matrix.

Also, the morphological characteristics of the TiNCu films were analyzed through the top-view and cross-sectional

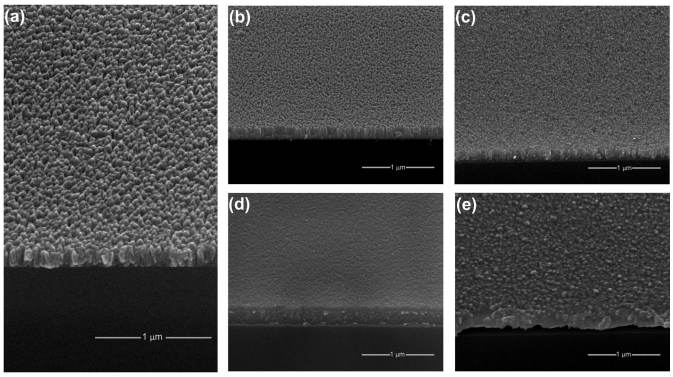

Fig. 3. SEM micrographs exhibiting the top-view surface for the thin films of (a) Ti, (b) TiN, (c) TiNCu, (d) TiCu, and (e) Cu.

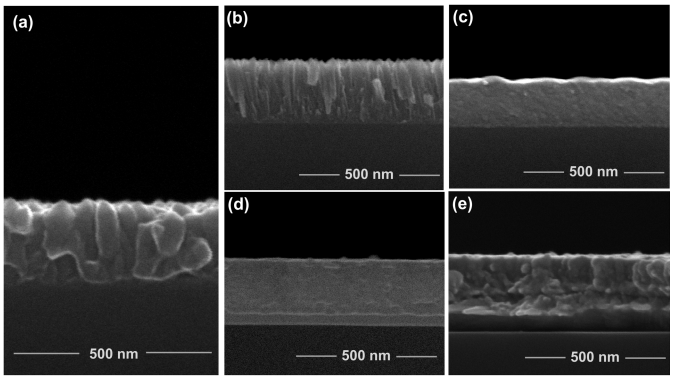

Fig. 4. SEM micrographs showing the cross section for the growth of the thin films of (a) Ti, (b) TiN, (c) TiNCu, (d) TiCu, and (e) Cu.

micrographs, presented in Figs. 3 and 4. The pure metallic Ti thin film exhibits a columnar-like growth, very common for physical depositions processed at low temperatures due to the lack of thermodynamic equilibrium conditions [Fig. 4(a)], which is also responsible for the observed rough surface [Fig. 3(a)]. Similar behavior is presented by the TiN thin film where the columnar growth [Fig. 4(b)] and the 3-D hexagonal grain features [Fig. 3(b)] are still present although less evident. The surface roughness phenomenon evolves significantly to smother surfaces when the Ti and TiN matrices are doped with copper, very close to what can be observed for the surface of the Cu thin film [Fig. 3(b)–(d)].

The addition of Cu to Ti and TiN also leads to the formation of denser featureless microstructures, with some shear striations and partially vein-like features [Fig. 4(c)], particularly evident for the TiCu thin film [Fig. 4(c)], typically associated with the fracture of metallic glassy samples, attesting the TFMG behavior reported for these films [11], [13]. A distinct microstructural evolution was developed by the Cu film [Figs. 3(d) and 4(d)], as the fracture spotlights the unique ductile behavior of the pure Cu thin film.

IV. EMG BIOPOTENTIAL ACQUISITION

A. Hardware and Software

To test the new system of dry, polymeric-based electrodes, EMG signals were acquired and analyzed from the bicep muscle (see Fig. 5). An NI 9234 signal acquisition system was coupled with LabVIEW software and was utilized for this

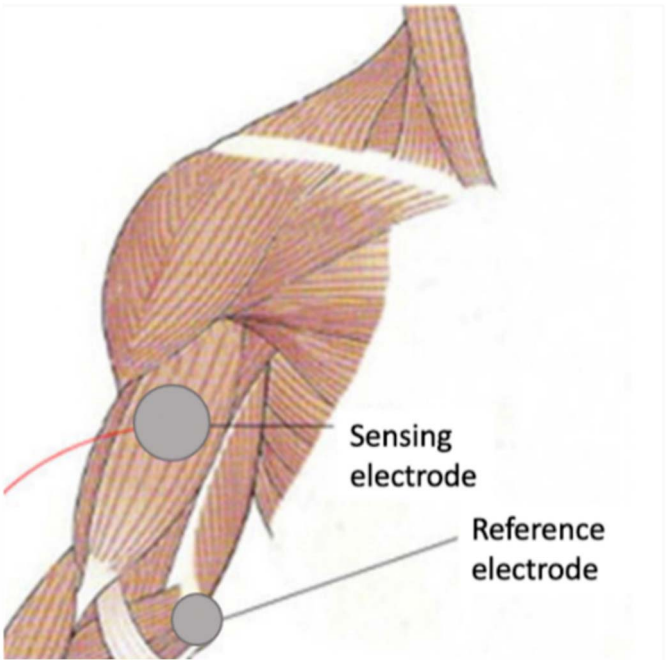

Fig. 5. Electrode placement for initial EMG acquisition.

data acquisition. Each pair of electrodes was attached from the bicep muscle and the elbow as a ground reference, shown in Fig. 5, to the NI 9234 device.

No external hardware amplifiers or filters were used in this process. Through LabVIEW, muscle signals were acquired, passed through a low-pass filter of 20 Hz to reduce noise, and displayed in a waveform graph. Real-time voltage versus time data was acquired at both resting states and muscle contraction states. We defined the resting state to be when the arm and the bicep muscle were relaxed. On the contrary, the contraction state was when the bicep muscle was contracted through an arm curling motion with a known weight [29], [30], [31]. Collected data could be observed immediately through the waveform graph and then converted to a readable data file for further analysis such as analyzing the noise at the resting state or observing the peak-to-peak voltages during the contraction state [29], [30], [31].

B. EMG Comparison of Substrates

First, all substrates (PU, PLA, and cellulose) were analyzed with all five films (Ti, Cu, TiN, TiCu, and TiNCu). Each pair of electrodes was attached to the bicep muscle and data acquisition system as previously mentioned. All tests were conducted procedurally. Each trial was performed in 1-min intervals. During this time, the first 15 s are known as the resting state. In 15 s, no bicep curls were performed, and the arm remained in a relaxed position at the side of the standing human body. Following this, the remaining 45 s consisted of one bicep curl every 5 s with a constant known weight. This is referred to as the contraction state. Each electrode pair underwent three trials.

Following the signal acquisition, all collected data were converted to files consisting of two variables: voltage and time. Using MATLAB, the files were read in, and the average and standard deviation were calculated during the resting state.

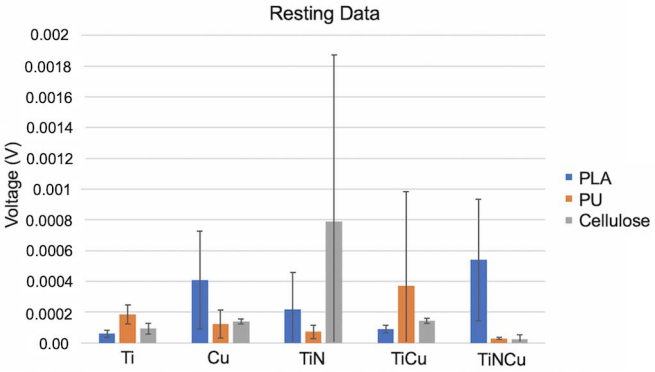

Fig. 6. Average noise during the resting state of electrodes with base substrates.

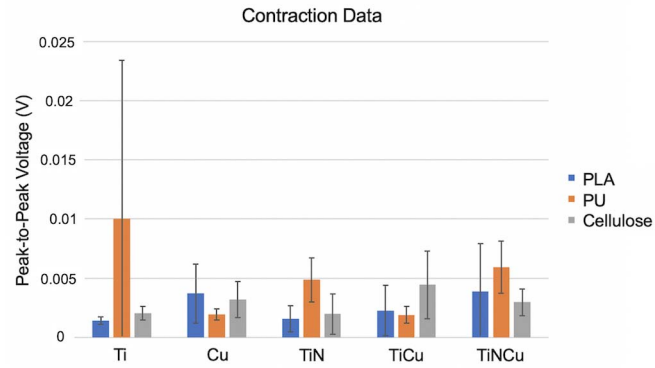

Fig. 7. Average peak-to-peak contraction values of electrodes with base substrates.

This allowed for observation of the noise of the electrodes and comparison between the different films and substrates. For the contraction segment of the signal, the peak-to-peak voltage, as well as the standard deviation, was calculated. Results for each of the substrates were averaged and compared through visual representations shown in Figs. 6 and 7.

C. EMG Comparison of Thin Films

Based on test results with all substrates and all thin films, evaluation was then narrowed down to only the PU substrate with all films. Electrodes were attached to the bicep indicated in Fig. 5 and attached to the NI9234 signal acquisition system. The same process of muscle relaxation/contraction was performed but was instead analyzed with three different weights. EMG biopotential signals were collected with the use of 2.27-, 6.80-, and 11.34-kg dumbbells for the contraction weight. Similarly, electrode pairs underwent three trials at each weight. Examples of the raw voltage versus time data for TiCu thin film with 2.27, 6.80, and 11.34 kg can be seen in the following.

Data were again exported to data files and analyzed through MATLAB, and the mean values, standard deviations, and peak-to-peak voltages were averaged. Fig. 9 shows how the contraction peak-to-peak voltages increased as bicep curl weight increased, which was expected. Due to an outlier in the TiNCu thin film data, the peak-to-peak voltage was lower at 11.34 kg in comparison to 6.80 kg. Because of this, the TiNCu thin film was not considered in further analysis.

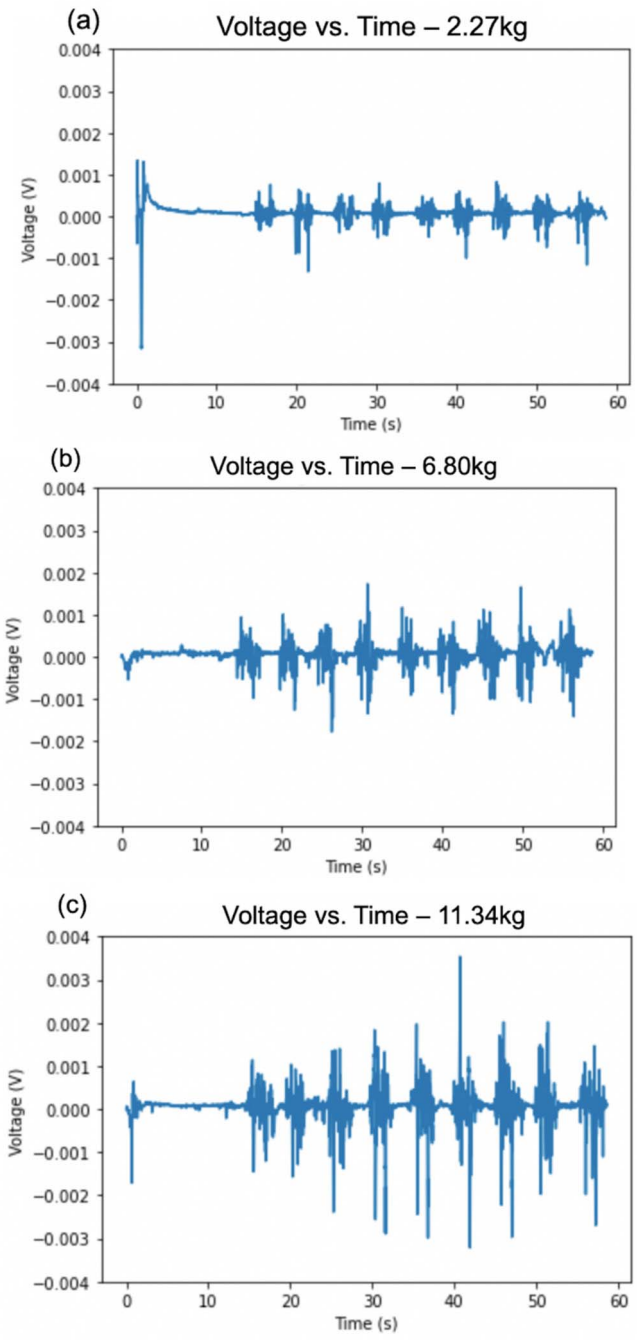

Fig. 8. Raw signals for TiCu thin film with contraction weights of (a) 2.27, (b) 6.80, and (c) 11.34 kg.

The increase in peak-to-peak voltage with increasing weight can more easily be seen represented as a line graph in Fig. 10.

From this graph, a sensitivity analysis was then performed to determine the limit of detection. In this case, the limit of detection is the smallest weight change needed to detect a reliable change in peak-to-peak voltage. The sensitivity of each thin film was determined by performing a linear regression analysis and calculating the slope on the peak-to-peak line graph. The noise collected for each thin film was calculated by analyzing the raw data during the resting state. Each resting data set was leveled off by subtracting the mean voltage from each data point. By doing this, the resulting mean would be 0 and data sets for each thin film could be combined. After concatenating the data for each film, the standard deviation was calculated and used as the noise for the limit of detection analysis. With these variables, the detection limit was found by using the equation 3.3*Noise/Sensitivity [32]. The constant 3.3 is used as a multiplication factor to account for a 90% confidence interval. A summary of the limit of detection calculation is described in Table II.

TABLE II
SUMMARY OF THE DETECTION LIMIT ANALYSIS

Thin Film	Sensitivity (mV/kg)	Noise (mV)	Detection Limit (kg) = 3.3*Noise/Sensitivity
Ti	1.995	0.414	0.685
TiN	0.287	0.0571	0.657
TiCu	0.595	0.106	0.588
Cu	1.823	0.390	0.706

Based on these results, the TiCu thin film was chosen for future work because it has the lowest limit of detection.

D. EMG Acquisition With an Amplifier

Following the limit of detection analysis, the TiCu thin film was used for further testing. To better observe the EMG biosignals and noise, a hardware amplifier and low-pass filter circuit were constructed. Electrodes were first attached to the bicep muscle, as shown in Fig. 11.

The electrodes were connected to a breadboard, with each one passing through a low-pass filter of 16 Hz. These signals were then passed through an AD 624 instrumentation amplifier set to a gain of 1000. A reference voltage of 2 V was used and the output of the amplifier was connected to the data acquisition system as previously mentioned. Like before, muscle signals were acquired through LabVIEW, passed through a software low-pass filter of 20 Hz, and displayed as a waveform graph. Real-time voltage versus time data was acquired at both resting states and muscle contraction states. The same process of muscle relaxation/contraction was performed and was again analyzed with weights of 2.27, 6.80, and 11.34 kg. Collected data were converted to readable excel files to estimate the average peak-to-peak voltages, standard deviation, and limit of detection with the addition of the amplifier and hardware filter. Similarly, the TiCu electrode pair underwent three trials at each weight. A summary of the increasing peak-to-peak voltages with weight is detailed in Fig. 12.

Using the same limit of detection procedure as detailed in Section III-B, we were able to use the sensitivity and the noise of the electrodes to determine the smallest change in weight that provided a reliable increase in voltage. A summary of these findings is indicated in Table III.

The results from the sensitivity analysis provide insight as to how the amplifier and filters affect the performance of the electrodes. With the addition of the hardware components, the detection limit increased from 0.588 to 3.32 kg. This is likely due to the fact that with the inclusion of the amplifier, external noise is also being amplified. This noise could possibly be reduced by including filters to remove noise from the power supply, but this needs to be further investigated [33].

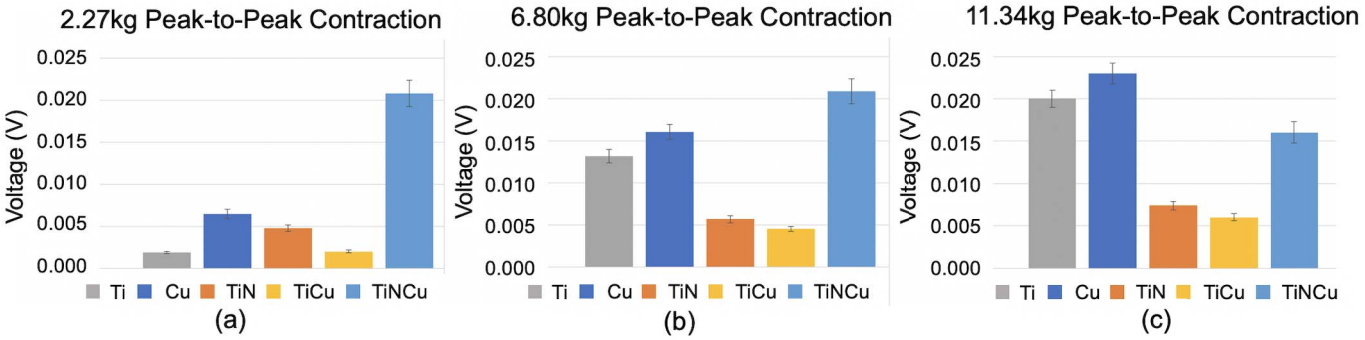

Fig. 9. Bar graphs representing peak-to-peak voltage for PU-based electrodes by increasing weights of (a) 2.27, (b) 6.80, and (c) 11.34 kg.

TABLE III
LIMIT OF DETECTION SUMMARY FOR THE TiCu THIN FILM

Thin Film	Sensitivity (mV/kg)	Noise (mV)	Detection Limit (kg) = 3.3*Noise/Sensitivity
TiCu	88.2	195	7.3

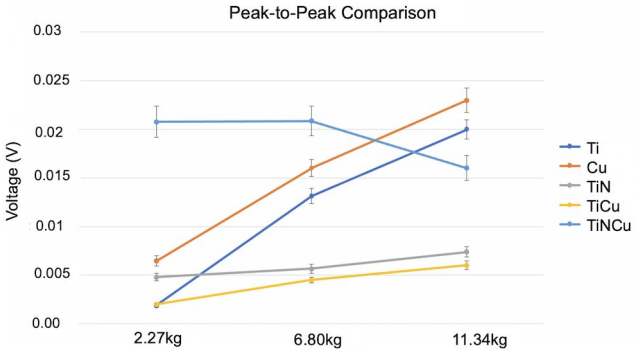

Fig. 10. Line graph representing peak-to-peak voltage with increasing weight for PU electrodes with respective thin films.

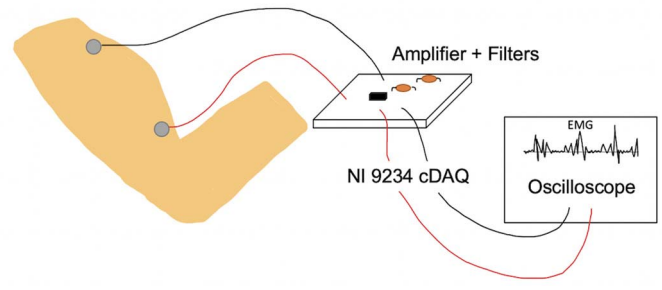

Fig. 11. Electrode placement for EMG acquisition and amplification.

V. MUSCLE STIMULATION

A. Electrical Stimulation Testing

One of our main goals in this study was to form a relationship between the EMG biosignals from the muscles and the amount of electrical stimulation that should be applied. To do this, we used a commercially available electrotherapy unit, the TENS 7000 2nd Edition Digital TENS Unit, to apply electrical stimulation and observe the crosstalk between the

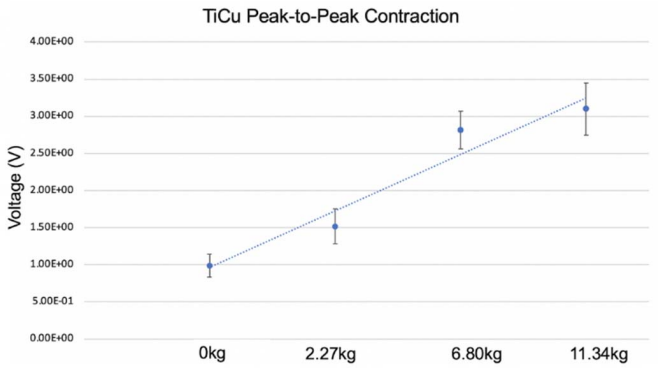

Fig. 12. TiCu peak-to-peak voltages with amplifier.

stimulating and sensing electrodes. This component of experimental testing was split into two parts. The first part consisted of attaching a pair of commercially available gel electrodes (stimulating electrodes) as well as a pair of TiCu PU dry electrodes (sensing electrodes) onto the bicep muscle, as shown in Fig. 13. The second testing segment implemented TiCu electrodes as both the sensing and stimulating electrodes. By doing this, we could compare the results with TiCu electrodes replacing the stimulating gel electrodes to analyze the noise of the system and observe how well the dry electrodes can stimulate without a gel interface. The TiCu electrodes with the PLA substrate were selected as stimulating electrodes for several reasons. We found that TiCu electrodes of the PU substrate with a diameter of 15 mm were not able to stimulate the bicep muscles. A tingling sensation could be felt at the highest output level of the TENS 7000 device, but no muscle contraction was visually observed. Electrodes of this substrate and thin film were not manufactured to larger sizes; thus, instead, we tested TiCu electrodes with a PLA base of 34 mm, so we were able to observe how a larger electrode interface would affect muscle contraction. With the 34-mm TiCu PLA electrodes, we could visualize muscle contraction at current levels similar to that of the commercial electrodes; therefore, we chose to use these electrodes as a stimulating pair to provide a comparison with the commercial ones.

The TENS 7000 unit can be controlled through an intensity control dial with levels ranging from 0 to 8. This intensity dial controls the pulse amplitude and the voltage output.

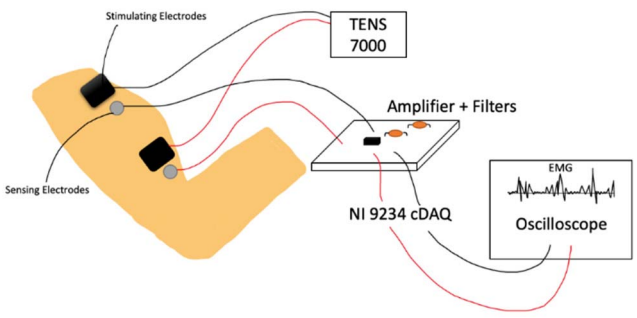

Fig. 13. Electrode placement for electrical stimulation and acquisition.

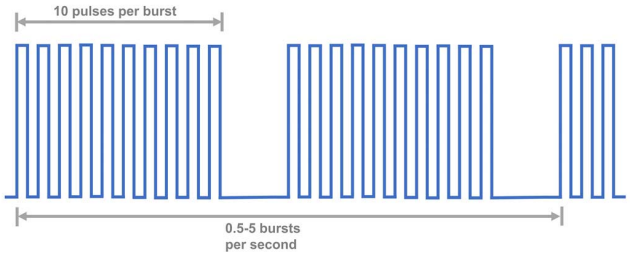

Fig. 14. TENS 7000 burst stimulation waveform.

The adjustable pulse amplitude ranges from 0 to 100 mA and the voltage output ranges from 0 to 50 V. Five stimulation modes (burst, normal, modulation, Strength-Duration 1, and Strength-Duration 2) were available to be selected as the source of stimulation. For our testing, we decided to stimulate with the burst mode: this stimulation form consists of a series of short, high-frequency pulses that are repeated at low-frequency time intervals. The waveform for this stimulation mode can be seen in Fig. 14. Other factors, such as the pulsewidth and pulse rate, could also be controlled and were increased to their highest setting, with the pulsewidth being 300 μs and the pulse rate being 5 Hz, to ensure capture and visibility on waveform graphs when signals were collected.

The procedures for each of the two portions of testing were the same. First, the electrodes (either commercial gel electrodes or TiCu on PLA electrodes) were taped onto the bicep. Then, the TiCu PU electrode pair was placed directly underneath the commercial pair ensuring no contact between the two. The electrode placement can again be seen in Fig. 13. Stimulating electrodes were attached to the TENS 7000 unit and sensing electrodes were connected to the low-pass filter and amplifier circuit, which was then connected to the NI 9234 compact data acquisition cDAQ unit for signal acquisition. Instead of using a dumbbell and a bicep curl to contract the muscle like in prior tests, the TENS 7000 unit was able to contract the muscle solely with electrical stimulation. Tests were performed at varying TENS 7000 levels with three trials per level. Each trial consisted of 30 s of signal acquisition. Tests began with the TENS 7000 unit turned off. At 5, 15, and 25 s, the unit was briefly turned on for approximately 2 s to the level being tested and turned off again to bring the muscle back to a relaxed state. The unit did not remain powered ON throughout the entirety of the trials to ensure

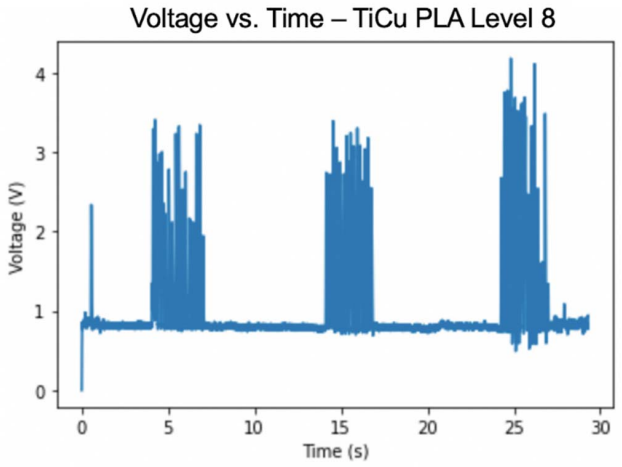

Fig. 15. EMG signal acquired from TiCu electrodes on PLA substrates with electrical stimulation applied at level 8.

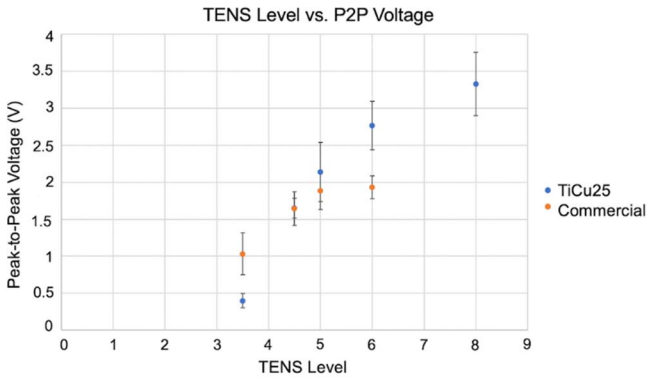

Fig. 16. TENS level versus contraction peak-to-peak voltages.

the visualization of distinct muscle contraction periods. Like before, data were collected through LabVIEW and exported as excel files for further analysis. It was observed that data across each trial were consistent; therefore, all data were included in the analysis. An example of this procedure displayed in a waveform graph is shown in Fig. 15.

B. Bicep Muscle Response to Electrical Stimulation

Following testing, EMG signals acquired from the TiCu sensing electrode pair were further examined and muscle contraction periods were divided to obtain average peak-to-peak and standard deviation values. Using the commercially available gel electrodes, it was evident that as the TENS 7000 output level increased, the bicep peak-to-peak contraction amplitude also increased, which was expected. Fig. 16 summarizes the biosignals acquired at different electrical stimulation levels with the use of commercial electrodes as the stimulating electrode pair. The peak-to-peak voltages corresponding to the muscular contraction at 5, 15, and 25 s are averaged for all three trials and standard deviations are calculated. In this, we can visualize this positive correlation between peak-to-peak voltage during contraction periods and the TENS 7000 level. It should be noted that tests only occurred up to a certain level with the commercial electrodes to ensure the comfort of the subject.

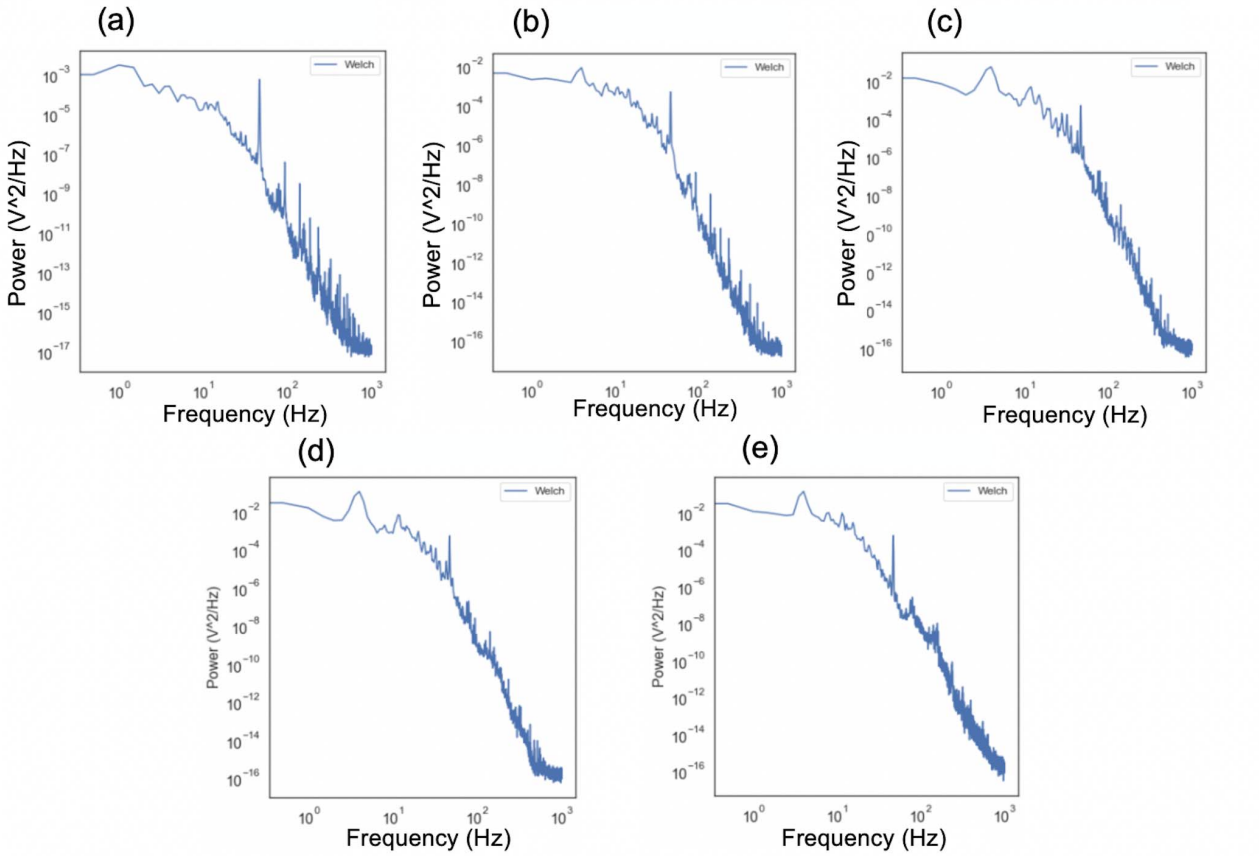

Fig. 17. PSD plots for acquired signals with TiCu at TENS level: (a) 3.5, (b) 4.5, (c) 5, (d) 6, and (e) 8.

EMG signals acquired from the TiCu sensing electrodes coupled with the pair of TiCu PLA stimulating electrodes were also analyzed. Similar to the commercial stimulating electrodes, it was indicated that as the TENS 7000 output level increased, the bicep contraction peak-to-peak also increased. This can be easily seen in Fig. 16 where there is a positive correlation between the TENS level and peak-to-peak contraction voltages. Performing tests with the TiCu PLA electrodes as the stimulating electrodes differed from the commercial electrodes because we were able to perform tests at the full current output while still maintaining comfort with the subject. Full current output correlates to level 8 on the TENS 7000 device and outputs a 100-mA current. Although it was unexpected that the TiCu PLA stimulating electrodes provided a higher peak-to-peak contraction voltage as the TENS level increased, we believe that the reasoning for this could be due to the fact that the electrode-to-skin interface is weaker than that of the commercial electrodes, thus leading to more noise in the system.

An analysis was performed through Python to examine the power spectral densities (PSDs) of the signals acquired through this series of tests to support the theory that at higher output levels, the noise increases. PSDs were estimated through Welch's method, which uses Fourier transforms to analyze the frequency domain of the signal. PSD plots were created for one signal acquired at each level (3.5, 4.5, 5, 6, and 8) and are shown in Fig. 17.

The area under each PSD plot provides an estimate of the variance of the acquired signal, directly correlating to the amount of noise. These areas were determined by integrating along the given axis using the composite trapezoidal rule and the results are summarized in Table IV. There is an evident increase in area as the TENS 7000 stimulation level increases, supporting the claim that as the level is increased, the noise in the system is also increased [34]. From these results, we can determine that there is some crosstalk between the stimulating and sensing electrodes, but this interference should be further investigated.

TABLE IV
PSD ANALYSIS AT VARYING TENS 7000 OUTPUT LEVELS

TENS 7000 Level	Area Under PSD Curve (V^2)
3.5	0.0042
4.5	0.0210
5	0.0894
6	0.1578
8	0.1937

VI. CONCLUSION

The main objective of this research was to develop and test the performance of dry surface electrodes of varying materials and substrates to determine an ideal electrode array for a future wearable rehabilitation device prototype. The substrate material and thin-film coating of sensors have a strong influence

on their biopotential sensing capabilities. Due to the specific experimental parameters and mechanisms involved in the sputtering deposition process, there is a deep connection between substrate characteristics and film growth, a factor that strongly conditions the final properties of the electrode. Therefore, the performance of dry surface electrodes of varying materials can be analyzed through muscular relaxation and contraction EMG acquisition tests to determine the most ideal material combination to be used in place of commercial gelled electrodes. EMG biosignals are important because they can assist in determining the correct level of electrotherapy to apply. Through applying functional electrical stimulation (FES), crosstalk between the stimulating electrodes and the signal acquiring electrodes can be determined, enabling design for state-of-the-art applications.

The work presented here addresses the need for home-based, easy-to-use FES devices to help treat those that suffer from mobility impairment. The first step in the development of such a system was the identification of the optimal electrode substrate and thin-film coating. A series of tests was performed by connecting electrodes to the bicep muscle group and collecting EMG biosignals during muscle relaxation and muscle contraction states. During the muscle relaxation state, the noise level could be further examined and compared between electrodes of varying substrates and films. Through muscular contractions, peak-to-peak voltages were acquired to compare the signal-to-noise ratio of the electrodes. Through the examination of all electrodes, the optimal substrate was first narrowed down. It was determined that the PU substrate, which is also the most flexible one, performed the best based on signal-to-noise ratio calculations. The PU substrate provided the highest signal-to-noise ratio because it is flexible that it adapts more easily to irregular body contours, thus making it ideal for further use. Following this, only the PU electrodes underwent additional testing to determine the best thin-film coating. From the acquired biosignals, a sensitivity analysis was performed to determine the detection limits for each thin-film material. The TiCu coating proved to have the lowest limit of detection, thus making it the most ideal thin film to use for signal acquisition.

Next, electrical stimulation was applied through commercially available gel electrodes as well as TiCu PLA electrodes. With electrical stimulation, muscle contraction was observed and analyzed through TiCu PU acquisition electrodes. Crosstalk between the stimulating and sensing electrodes was examined to ensure the proper performance of the system. As the electrical current applied was increased, the muscle activation also proved to increase based on signals collected. Results with TiCu PLA electrodes proved to be similar to those of the commercially available gel electrodes, and however, variability occurred as the TENS 7000 level increased. As the adjustable current amplitude level increased, it was noted that the peak-to-peak contraction voltage increased more with the TiCu PLA electrodes than with the commercial electrodes. This is likely due to the fact that the motion artifact between the TiCu PLA electrodes and the skin is weaker than the commercial electrode-to-skin interface, leading to an increase in the noise of the acquired signal.

This work has highlighted the advantages of dry surface electrodes to be used in place of commercial wet electrodes. The research proposed has shown the effectiveness of PU-based, TiCu-coated electrodes and how they are comparable to commercial electrodes. The electrodes involved in research can be applied to novel configurations used with FES devices and EMG acquisition.

REFERENCES

[1] *World Population Ageing 2020 Highlights: Living Arrangements of Older Persons*, United Nations Department of Economic and Social Affairs, New York, NY, USA, 2020.

[2] J. van Vuuren et al., "Reshaping healthcare delivery for elderly patients: The role of community paramedicine; a systematic review," *BMC Health Serv. Res.*, vol. 21, no. 1, p. 29, 2021, doi: 10.1186/S12913-020-06037-0.

[3] J. Alwin, B. W. Karlson, M. Husberg, P. Carlsson, and N. Ekerstad, "Societal costs of informal care of community-dwelling frail elderly people," *Scandin. J. Public Health*, vol. 49, no. 4, pp. 433–440, Dec. 2019, doi: 10.1177/1403494819844354.

[4] L. Forma, M. Aaltonen, J. Pulkki, J. Raitanen, P. Rissanen, and M. Jylhä, "Long-term care is increasingly concentrated in the last years of life: A change from 2000 to 2011," *Eur. J. Public Health*, vol. 27, no. 4, pp. 665–669, Aug. 2017, doi: 10.1093/EURPUB/CKW260.

[5] *Decade of Healthy Ageing: Baseline Report*, World Health Organization, Geneva, Switzerland, 2020.

[6] C. Cunningham, R. O. Sullivan, P. Caserotti, and M. A. Tully, "Consequences of physical inactivity in older adults: A systematic review of reviews and meta-analyses," *Scandin. J. Med. Sci. Sports*, vol. 30, no. 5, pp. 816–827, May 2020, doi: 10.1111/SMS.13616.

[7] R. Fejer and A. Ruhe, "What is the prevalence of musculoskeletal problems in the elderly population in developed countries? A systematic critical literature review," *Chiropractic Manual Therapies*, vol. 20, no. 1, p. 31, Dec. 2012, doi: 10.1186/2045-709X-20-31.

[8] A. Cieza, K. Causey, K. Kamenov, S. W. Hanson, S. Chatterji, and T. Vos, "Global estimates of the need for rehabilitation based on the global burden of disease study 2019: A systematic analysis for the global burden of disease study 2019," *Lancet*, vol. 396, no. 10267, pp. 2006–2017, Dec. 2020, doi: 10.1016/S0140-6736(20)32340-0.

[9] A. Faragli et al., "The role of non-invasive devices for the telemonitoring of heart failure patients," *Heart Failure Rev.*, vol. 26, no. 5, pp. 1063–1080, 2021, doi: 10.1007/S10741-020-09963-7.

[10] X. Niu, X. Gao, Y. Liu, and H. Liu, "Surface bioelectric dry electrodes: A review," *Measurement*, vol. 183, Oct. 2021, Art. no. 109774, doi: 10.1016/J.MEASUREMENT.2021.109774.

[11] C. Lopes et al., "Me-doped Ti–Me intermetallic thin films used for dry biopotential electrodes: A comparative case study," *Sensors*, vol. 21, no. 23, p. 8143, Dec. 2021, doi: 10.3390/S21238143.

[12] M. S. Rodrigues et al., "Dry electrodes for surface electromyography based on architectured titanium thin films," *Materials*, vol. 13, no. 9, p. 2135, May 2020, doi: 10.3390/MA13092135.

[13] C. Lopes et al., "Evolution of the mechanical properties of Ti-based intermetallic thin films doped with different metals to be used as biomedical devices," *Appl. Surf. Sci.*, vol. 505, Nov. 2019, Art. no. 144617, doi: 10.1016/J.APSUSC.2019.144617.

[14] M. R. Akbarpour and S. M. Javadhesari, "Wear performance of novel nanostructured Ti-Cu intermetallic alloy as a potential material for biomedical applications," *J. Alloys Compounds*, vol. 699, pp. 882–886, Mar. 2017, doi: 10.1016/J.JALLCOM.2017.01.020.

[15] C. Lopes et al., "Multifunctional Ti–Me (Me = Al, Cu) thin film systems for biomedical sensing devices," *Vacuum*, vol. 122, pp. 353–359, Dec. 2015, doi: 10.1016/J.VACUUM.2015.05.015.

[16] P. Pedrosa et al., "Ag:TiN-coated polyurethane for dry biopotential electrodes: From polymer plasma interface activation to the first EEG measurements," *Plasma Process. Polym.*, vol. 13, no. 3, pp. 341–354, Mar. 2016, doi: 10.1002/PPAP.201500063.

[17] M. J. Lima et al., "Modification of steel surfaces with nanometer films of Al_2O_3 and TiO_2 decreases interfacial adhesion to polymers: Implications for demolding shape-engineered polymer products," *ACS Appl. Nano Mater.*, vol. 4, no. 10, pp. 10018–10028, Oct. 2021, doi: 10.1021/ACSANM.1C00995.

[18] F. M. Fowkes, "Attractive forces at interfaces," *Ind. Eng. Chem.*, vol. 56, no. 12, pp. 40–52, Dec. 1964, doi: 10.1021/IE50660A008.

[19] R. Tyagi, A. K. Das, and A. Mandal, "Wettability and performance of Cu-MoS_2/SiC coating prepared by electro-discharge coating process," *Trans. Indian Inst. Met.*, vol. 75, no. 6, pp. 1563–1572, Jun. 2022, doi: 10.1007/S12666-022-02531-7.
[20] A. Holländer and J. Thome, "Degradation and stability of plasma polymers," in *Plasma Polymer Films*. Singapore: World Scientific, 2004, pp. 247–277.
[21] N. P. Barradas and C. Jeynes, "Advanced physics and algorithms in the IBA DataFurnace," *Nucl. Instrum. Methods Phys. Res. B, Beam Interact. Mater. Atoms*, vol. 266, no. 8, pp. 1875–1879, Apr. 2008, doi: 10.1016/J.NIMB.2007.10.044.
[22] N. P. Barradas, E. Alves, C. Jeynes, and M. Tosaki, "Accurate simulation of backscattering spectra in the presence of sharp resonances," *Nucl. Instrum. Methods Phys. Res. B: Beam Interact. Mater. Atoms*, vol. 247, no. 2, pp. 381–389, Jun. 2006, doi: 10.1016/J.NIMB.2006.02.004.
[23] D. Morais et al., "Bioactive and biopassive treatment of poly(ethylene terephthalate) multifilament textile yarns to improve/prevent fibroblast viability," *J. Biomed. Mater. Res. B, Appl. Biomater.*, vol. 2020, p. 34882, May 2021, doi: 10.1002/JBM.B.34882.
[24] M. Fazeli, J. P. Florez, and R. A. Simão, "Improvement in adhesion of cellulose fibers to the thermoplastic starch matrix by plasma treatment modification," *Compos. B, Eng.*, vol. 163, pp. 207–216, Apr. 2019, doi: 10.1016/J.COMPOSITESB.2018.11.048.
[25] D. Packham, "Surface energy, surface topography and adhesion," *Int. J. Adhes. Adhesives*, vol. 23, no. 6, pp. 437–448, Jan. 2003, doi: 10.1016/S0143-7496(03)00068-X.
[26] A. Davoodi, H. H. Zadeh, M. D. Joupari, M. A. Sahebalzamani, M. R. Khani, and S. Shahabi, "Physicochemical- and biocompatibility of oxygen and nitrogen plasma treatment using a PLA scaffold," *AIP Adv.*, vol. 10, no. 12, Dec. 2020, Art. no. 125205.
[27] G. Zhao, J. Gao, Q. Gao, and Y. Chen, "Surface modification of biodegradable poly(D,L-lactic acid) by nitrogen and nitrogen/hydrogen plasma for improving surface hydrophilicity," *Plasma Sci. Technol.*, vol. 13, no. 2, pp. 230–234, Apr. 2011, doi: 10.1088/1009-0630/13/2/20.
[28] R. Morent et al., "Influence of discharge atmosphere on the ageing behaviour of plasma-treated polylactic acid," *Plasma Chem. Plasma Process.*, vol. 30, no. 4, pp. 525–536, 2010, doi: 10.1007/S11090-010-9233-8.
[29] N. U. Ahamed, K. Sundaraj, M. Alqahtani, O. Altwijri, M. A. Ali, and M. A. Islam, "EMG-force relationship during static contraction: Effects on sensor placement locations on biceps Brachii muscle," *Technol. Health Care*, vol. 22, no. 4, pp. 505–513, Aug. 2014, doi: 10.3233/THC-140842.
[30] J. C. Carr, T. W. Beck, X. Ye, and N. P. Wages, "Intensity-dependent EMG response for the biceps brachii during sustained maximal and submaximal isometric contractions," *Eur. J. Appl. Physiol.*, vol. 116, no. 9, pp. 1747–1755, Sep. 2016, doi: 10.1007/S00421-016-3435-6.
[31] A. B. Yahya, W. M. B. W. Daud, C. S. Horng, and R. Sudirman, "Electromyography signal on biceps muscle in time domain analysis," *J. Mech. Eng. Sci.*, vol. 7, pp. 1179–1188, Dec. 2014, doi: 10.15282/JMES.7.2014.17.0115.
[32] M. Halim. (2021). *Re: How to Calculate the Detection Limit From the Calibration Curve?* [Online]. Available: https://www.researchgate.net/post/How-to-calculate-the-detection-limit-from-the-calibration-curve/616c0c16e3927400ea229935/citation/download
[33] R. Mancini, *Op Amps for Everyone*. Amsterdam, The Netherlands: Elsevier, 2018.
[34] R. H. Chowdhury, M. B. I. Reaz, M. A. B. M. Ali, A. A. A. Bakar, K. Chellappan, and T. G. Chang, "Surface electromyography signal processing and classification techniques," *Sensors*, vol. 13, no. 9, pp. 12431–12466, Sep. 2013, doi: 10.3390/S130912431.

Cláudia Lopes was born in Hilden, Düsseldorf, Germany, in 1978. She received the B.Sc. degree in physics and chemistry and the M.Sc. and Ph.D. degrees in physics from the University of Minho, Braga, Portugal, in 2003, 2009, and 2018, respectively.

She has been working in materials science research and development since 2011, developing and optimizing nanostructured thin films (by physical vapor deposition (PVD) processes) for sensing. Since 2020, she has been a Research Scientist at the Center of Physics, University of Minho, and the University of Porto, Porto, Portugal, working on dry and flexible sensors to be integrated into wearables. She has experience in the biomedical field, leading multidisciplinary projects in the area, with clinical trials for in vivo testing.

Hugo Veloso received the B.Sc. degree in technological physics and the M.Sc. degree in physics engineering, with a specialization in optical physics, from the Faculty of Science, University of Porto, Porto, Portugal, in 2020. His master's thesis, regarding the optimization of laser induced breakdown spectroscopy (LIBS) analysis in the cork industry, was developed in partnership with the Centre of Applied Photonics, INESC TEC, Porto, Portugal.

He was a Collaborating Researcher with the Centre of Applied Photonics, INESC TEC, from 2019 to 2021.

Makenna Hayes received the B.Sc. degree in mechanical engineering from The University of Texas at Austin (UT Austin), Austin, TX, USA, in 2021, and the M.Sc. degree in mechanical engineering, with a focus on biomechanical engineering, from UT Austin in 2022.

From 2021 to 2022, she worked as a Graduate Research Assistant at the Nanoscale Design and Manufacturing Laboratory, UT Austin. Her research centered on testing the performance of dry, flexible biopotential electrodes to be integrated into wearable rehabilitation devices.

Michael A. Cullinan (Member, IEEE) received the B.S. degree in engineering and the B.A. degree in economics from the Swarthmore College, Swarthmore, PA, USA, in 2006, and the M.S. and Ph.D. degrees in mechanical engineering from the Massachusetts Institute of Technology, Cambridge, MA, USA, in 2008 and 2011, respectively.

He is currently an Associate Professor and the Director of the Nanoscale Design and Manufacturing Laboratory, The University of Texas at Austin, Austin, TX, USA. Prior to joining The University of Texas at Austin, he was a National Research Council Postdoctoral Associate with the National Institute of Standards and Technology, Gaithersburg, MD, USA. His research interests include the design and development of nanomanufacturing processes and equipment, the application of nanoscale science in engineering, the engineering of thin films, nanotubes and nanowires, the manufacturing and assembly of nanostructured materials, and the design of microscale/nanoscale machine elements for mechanical sensors and energy systems.

Filipe Vaz received the B.Sc. degree in physics and chemistry, the Ph.D. degree in physics, and the Habilitation degree from the University of Minho, Braga, Portugal, in 1992, 2000, and 2012, respectively.

He has supervised 12 Postdocs, 14 Ph.D. students, and 41 M.Sc. students. The main research topics concern nanostructured thin films for sensing applications, and optical thin-film systems and films with localized surface plasmon resonance behavior. He participated as a coordinator/collaborator in 19 National projects, ten European projects as a National coordinator, and 12 European bilateral projects as a coordinator. He has coauthored 250 aritcles in refereed international journals (Scopus—H index of 40, >5200 citations) and three patents.